Structural Basis for Substrate Specificity in Group I Nucleoside Hydrolases[†,‡]

Elena Iovane,[§,||] Barbara Giabbai,[§,||,⊥] Laura Muzzolini,[§] Vittoria Matafora,[#] Arianna Fornili,[§] Claudia Minici,[§] Francesca Giannese,[§] and Massimo Degano*[,§]

Biocrystallography Unit and Mass Spectrometry Unit, DIBIT San Raffaele Scientific Institute, via Olgettina 58, 20132 Milan, Italy

Received December 15, 2007; Revised Manuscript Received February 20, 2008

ABSTRACT: Enzymes with nucleoside hydrolase activity (NHs) belonging to homology group I either are markedly specific for pyrimidine nucleoside substrates or hydrolyze with comparable efficiencies the N-glycosidic bond in all common nucleosides. The biochemical and structural basis for these differences in substrate specificity is still unknown. Here we characterize the binding interactions between the slowly hydrolyzed substrate inosine and the *Escherichia coli* pyrimidine-specific NH YeiK using cryotrapping and X-ray crystallography. Guided by the structural features of the Michaelis complex, we show the synergic effect of two specific point mutations in YeiK that increase the catalytic efficiency toward purine nucleosides to values comparable to those of natural nonspecific NHs. We demonstrate that the integrity of an active-site catalytic triad comprised of two hydroxylated amino acids and one histidine residue is a requirement for the highly efficient hydrolysis of inosine by group I NHs. Instead, cleavage of the YeiK-preferred substrate uridine is not affected by mutations at the same locations, suggesting a different fine chemical mechanism for the hydrolysis of the two nucleoside substrates. Our study provides for the first time direct evidence that distinct subsets of amino acid residues are involved in the hydrolysis of purine or pyrimidine nucleosides in group I NHs.

Nucleoside hydrolases are widespread Ca^{2+}-dependent metalloenzymes that efficiently catalyze the hydrolytic excision of the N-glycosidic bond in nucleosides (*1, 2*). Their biological function is well-established in purine-auxotrophic protozoa such as trypanosomes, where they are involved in the recycling pathway of nitrogenous bases for subsequent nucleotide synthesis (*3*). Because of their central role in providing these essential building blocks for the parasite life cycle, NHs[1] are considered attractive targets for rational drug design (*1*). On the other hand, the functional role performed by NHs in prokaryotes and higher eukaryotes is still debated, and existing data point to highly specialized and diverse functions such as prevention of sporulation in *Bacillus subtilis* (*4*) or reduction of the perception of micropredation by the mosquito *Aedes aegypti* (*5*). Recent results linked the uridine hydrolase from the yeast *Saccharomyces cerevisiae* to the metabolism of the nucleoside nicotinamide riboside in NAD^+ homeostasis. These studies implicated a role of the yeast hydrolase in elevating NAD^+ levels in calorie restriction, and in extending the lifespan through a Sir2-dependent mechanism (*6*). While it is yet unknown whether the bacterial enzymes may be involved in similar cellular mechanisms, these findings raise the provocative possibility that NHs could be active in biochemical pathways alternative to nucleotide catabolism. These functional studies require a parallel detailed definition of the biochemical and structural properties of NHs.

Enzymes with NH activity are classified on the basis of their substrate specificity as purine-specific (IAG-NH) (*7, 8*), nonspecific (IU-NH) (*9*), pyrimidine-specific (CU-NH) (*10*), and 6-oxopurine-specific (GI-NH) (*11*). NHs can be also grouped according to sequence homology and conservation of active-site residues (*10*). This classification allows the immediate distinction between pyrimidine- and purine-specific enzymes based upon the presence of either a histidine or a tryptophan residue at a critical active-site position (*10*). However, homology group I includes both nonspecific and pyrimidine-specific NHs, which share a high degree (30–70%) of sequence identity but have distinct substrate specificities. Indeed, while IU-NHs cleave the N-glycosidic bond in both purine and pyrimidine nucleosides with comparable catalytic efficiencies, CU-NHs show 10^2-10^4-fold faster hydrolysis of cytidine or uridine compared to purine nucleosides (*10, 12*). The biochemical and structural basis for these differences in substrate specificity is yet to be clarified. One possibility is that IU-NHs are acquired-function mutants of CU-NHs, and specific amino acids are present to stabilize the transition

[†] This work was supported by research grants from Italian Basic Research Funding (FIRB), Fondazione Cariplo, and the Italian Association for Cancer Research (AIRC).

[‡] The coordinates and structure factors of the YeiK−inosine complex have been deposited with the Protein Data Bank as entry 3B9X.

* To whom correspondence should be addressed. Telephone: +39 022643-7152. Fax: +39 022643-4153. E-mail: degano.massimo@hsr.it.

[§] Biocrystallography Unit.

[||] These authors contributed equally to this work.

[⊥] Present address: AdriaCell Srl, AREA Science Park, S.S. 14 km 163, 5, I-34012 Trieste-Basovizza (TS), Italy.

[#] Mass Spectrometry Unit.

[1] Abbreviations: NH, nucleoside hydrolase; IU-NH, inosine-uridine-preferring nucleoside hydrolase; CU-NH, cytidine-uridine-preferring nucleoside hydrolase; IAG-NH, inosine-adenosine-guanosine-preferring nucleoside hydrolase; GI-NH, guanosine-inosine-preferring nucleoside hydrolase; pAPIR, 1-(4-amino-phenyl)-2-(hydroxymethyl)pyrrolidine-3,4-diol; Hepes, 4-(2-hydroxyethyl)-1-piperazineethanesulfonic acid; PEG, polyethylene glycol; YY, Thr223Tyr/Gln227Tyr double mutant of YeiK; FY, Thr223Phe/Gln227Tyr double mutant of YeiK.

10.1021/bi702448s CCC: $40.75
Published on Web 03/25/2008

state for purine nucleoside hydrolysis. Alternatively, CU-NH enzymes could be endowed with specific active-site features that selectively discriminate the leaving group of pyrimidine nucleosides. Kinetic isotope effect studies on the IU-NH from *Crithidia fasciculata* demonstrated that the NH-catalyzed cleavage of inosine proceeds through the distortion of substrate toward an oxonium cation geometry via ground-state destabilization (*13*). A partial negative charge develops at the nitrogenous base, and protonation of the leaving group is thus required for efficient catalysis. A conserved active-site histidine is a likely candidate for this role (*14*). Also, it is still unknown whether the same strategy is used for the stabilization of the negative charge in the NH-catalyzed purine and pyrimidine nucleoside hydrolysis. In this work, we address these open questions through the crystallographic characterization of the Michaelis complex between the CU-NH YeiK (RihB) from *Escherichia coli* and inosine, and site-directed mutagenesis (*10, 15*). We engineered two specific active-site mutations that elicit a 50-fold increase in catalytic efficiency of the enzyme toward inosine, demonstrating that IU-NHs are characterized by a catalytic triad, composed of one histidine and two tyrosine residues, allowing the efficient protonation of the purine base. Surprisingly, the mutations introduced into the YeiK enzyme did not affect the hydrolysis of uridine, suggesting that these residues are employed differently by the homologous CU- and IU-NH enzymes for the hydrolysis of purine and pyrimidine nucleosides.

MATERIALS AND METHODS

Site-Directed Mutagenesis of YeiK. The single-amino acid mutants T223A, T223F, T223Y, Q227A, Q227F, and Q227Y and the double mutants T223F/Q227Y (termed FY) and T223Y/Q227Y (YY) were generated using polymerase chain reaction (PCR) with the proofreading Pfu DNA polymerase. Single-point mutants were generated from the pET28-YEIK template, bearing the K12 *E. coli yeiK* gene (*16*). Reaction mixtures were primed with two complementary mutagenic oligonucleotides, designed to include the desired mutation at the central codon, at a concentration of 1 μM. The FY and YY double mutants were generated by introducing the second Q223Y or T223Y mutation on the pET28 vector bearing the T223F or Q227Y variant of the YeiK gene. PCRs with a hot start protocol were carried out by cycles of denaturation at 94 °C, annealing, and extension at 68 °C. The annealing temperature and the number of cycles in the reaction were optimized according to the number of bases to be mutated (Table 1). A final extension for 15 min at 72 °C was included for all mutants. The parental permethylated DNA was digested with the endonuclease *Dpn*I (*17*). The reaction product, corresponding to the mutated nicked plasmid DNA, was purified using PCRQuick spin columns (Promega) prior to transformation, to improve the efficiency, into chemically competent TOP10 *E. coli* cells. Plasmid DNA was isolated from single colonies and sequenced on both DNA strands using the automated dideoxy method.

Expression and Purification of YeiK and Its Variants. Wild-type and mutated YeiK were overexpressed in *E. coli* BL21(DE3) cells and purified as previously described using NiNTA affinity and size exclusion chromatography (*16*). The N-terminal hexahistidine tag was cleaved from the enzymes via quantitative digestion using thrombin in a 1:1000 (w/w) ratio and separated via size exclusion chromatography. The quantitative incorporation of the desired mutation(s) into the purified protein was verified through partial proteolysis with trypsin, followed by MALDI-TOF mass spectrometric analysis of the resulting peptide mixture. The protein concentration was determined using the following molar absorption coefficients at 280 nm: 23.3 $mM^{-1}\cdot cm^{-1}$ for YeiK wild-type, 22.9 mM^{-1} cm^{-1} for T223A, 22.9 mM^{-1} cm^{-1} for T223F, 24.4 mM^{-1} cm^{-1} for T223Y, 22.9 mM^{-1} cm^{-1} for Q227A, 22.9 mM^{-1} cm^{-1} for Q227F, 24.2 mM^{-1} cm^{-1} for Q227Y, 24.4 mM^{-1} cm^{-1} for FY, 25.0 mM^{-1} cm^{-1} for YY, and 22.5 mM^{-1} cm^{-1} for H239A.

Table 1: Oligonucleotides Used for Site-Directed Mutagenesis of YeiK[a]

mutant	sequence	T_{anneal} (°C)	no. of PCR cycles
T223A	CATCATGAACTTCGCTCTCAAAACGCAG	55	12
T223F	CATCATGAACTTCTTTCTCAAAACGCAG	54	16
T223Y	CGACATCATGAACTTCTATCTCAAAACG	55	16
Q227A	CTCTCAAAACGGCGTTCGAAAACTAC	54	16
Q227F	CACTCTCAAAACGTTCTTCGAAAACTAC	54	16
Q227Y	CACTCTCAAAACGTATTTCGAAAACTAC	55	16
FY	CTTCTCAAAACGTATTTCGAAAACTACG	54	16
YY	CGACATCATGAACTTCTATCTCAAAACG	55	16

[a] The mutated bases are underlined in the nucleotide sequence. The mutagenic PCR was carried out using the indicated oligonucleotide and one corresponding to the complementary and inverse sequence. For the FY and YY double mutants, the indicated oligonucleotide was used to introduce a second mutation into the T223F and Q227Y mutants, respectively.

Cloning, Expression, and Purification of URH1p from S. cerevisiae. The *urh1* gene was cloned using PCR from genomic *S. cerevisiae* DNA. Forward and reverse primers based on the deposited gene sequence (GenBank accession number 37362635) were engineered to contain *Nhe*I and *Xho*I restriction sites at the 5′- and 3′-ends, respectively. The proofreading Pfu DNA polymerase was employed to prevent nucleotide misincorporation. The PCR product was directionally cloned in the TOPO-pET101 vector (Invitrogen) and sequenced on both DNA strands. The *urh1* gene was then subcloned between the *Nhe*I and *Xho*I sites of a pET28b vector. The pET28-URH1 plasmid was transformed in *E. coli* Rosetta(DE3) cells for protein production. An overnight bacterial culture was diluted 1:10 in Luria-Bertani broth containing 1% glucose, 50 μg/mL kanamycin, and 34 μg/mL chloramphenicol and grown under vigorous shaking (210 rpm) to an OD_{600} of 0.6. The culture was cooled to 20 °C, and protein expression was induced by addition of isopropyl β-D-thiogalactopyranoside to a final concentration of 0.25 mM. Cells were harvested by centrifugation after 16 h, resuspended in a buffer containing 20 mM Tris (pH 8.0), 50 mM NaCl, and Complete EDTA-free protease inhibitors (Roche), and lysed using a Bandelin sonifier. The supernatant was mixed for 3 h at room temperature with NiNTA resin (350 μL/L of cell culture) and packed onto a polypropylene column, and unbound proteins were removed by extensive washing with 20 mM Tris (pH 8.0), 500 mM NaCl, and 10 mM imidazole. Bound URH1p was eluted by increasing the imidazole concentration of 500 mM. The protein was dialyzed against a buffer composed of 20 mM Tris (pH 8.4), 150 mM NaCl, and 2.5 mM $CaCl_2$ and incubated with a 1:200 (w/w) solution of bovine thrombin (Sigma) for 16 h at 4 °C. URH1p was dialyzed overnight in 20 mM Tris (pH 7.5), loaded onto a MonoQ anion exchange column, and

eluted with a linear KCl gradient. The protein concentration was determined using the BCA assay (Pierce). Quantitative removal of the affinity tag was assessed by Western blotting with an anti-hexahistidine antibody conjugated with horseradish peroxidase and luminol detection. Protein preparations were >95% pure, as judged from Coomassie-stained SDS−PAGE.

Steady-State Kinetic Analysis. Kinetic parameters for wild-type YeiK, site-specific mutants, and URH1p were determined using a colorimetric or spectrophotometric assay. The NH colorimetric test based on the reducing sugar assay was performed as previously described (*9*). Kinetic measurements were recorded on a UltroSpec UV spectrophotometer, monitoring continuously the variation in absorbance at the appropriate wavelengths (for uridine, at 280 nm, $\Delta\epsilon = -2.0$ μM^{-1} cm^{-1}; for inosine, at 280 nm, $\Delta\epsilon = -0.82$ μM^{-1} cm^{-1}). The concentration of substrate was varied between $0.1K_M$ and $10K_M$, and initial velocities were measured for a minimum of eight points. Enzymatic reactions were performed in 50 mM Hepes buffer (pH 7.3) at 37 °C. Kinetic parameters were obtained via a direct fit to initial velocities to the Michaelis–Menten equation using GraphPad Prism. All kinetic parameters are calculated per active site, and they were, thus, independent of the multimerization state of the enzyme.

X-ray Crystallography. Wild-type YeiK at 8–9 mg/mL in 20 mM Hepes (pH 7.4) and 150 mM NaCl was crystallized using the hanging drop vapor diffusion method, mixing equal volumes of protein solution and a precipitant solution consisting of 100 mM Tris (pH 8.5), 200 mM NaCl, and 24% PEG 4000. A single crystal was harvested and equilibrated into a stabilizing solution containing 100 mM Hepes (pH 8.5), 200 mM NaCl, and 34% PEG 4000. The crystal was then transferred for 2 min in the same solution containing 50 mM inosine, mounted on a fiber loop, and immediately dipped into liquid nitrogen. Diffraction data to 2.3 Å resolution were collected on a RAXIS-IV^{++} imaging plate detector coupled to a MicroMax007 X-ray generator with a copper target and Osmic optics using the oscillation method at 100 K. Data were indexed, integrated, scaled, and reduced to unique reflections with XDS (*18*). Since the crystal unit cell was chosen with a different setting (acute angles, as per IUCr guidelines) with respect to the deposited YeiK structure (Protein Data Bank entry 1Q8F), the orientation of the YeiK tetramer was determined using the molecular replacement method as implemented in MOLREP (*19*) after all ligand and water molecules had been removed. The structure was subjected to cycles of restrained energy minimization with a maximum likelihood target function using REFMAC5 (*20*) followed by manual rebuilding into σ_A-weighted electron density maps with COOT (*21*). Tight noncrystallographic symmetry restraints were maintained for the four YeiK chains present in the crystal cell. Because of structural differences, the restraints were set to medium and loose for residues 221−238 and 78−101, respectively. Residue Arg175 had different conformations in all molecules and was hence excluded from noncrystallographic symmetry restraints. Solvent molecules were added to the model using COOT. All residues in the refined model have dihedral angles (φ and ψ) belonging to the allowed regions of a Ramachandran plot. Details of data collection and final refinement statistics are presented in Table 2.

Table 2: Data Collection and Refinement Statistics[a]

Crystal Parameters	
unit cell	$a = 45.11$ Å, $b = 82.41$ Å, $c = 90.16$ Å, $\alpha = 67.90°$, $\beta = 79.59°$, $\gamma = 89.65°$
space group	*P*1
Data Collection	
wavelength (Å)	1.5418
resolution range (Å)	100–2.3 (2.45–2.3)
no. of unique reflections	50148 (5843)
completeness (%)	95.4 (92.6)
redundancy	7.3 (6.7)
$I/\sigma(I)$	18.7 (8.9)
R_{sym}[b]	0.095 (0.235)
R_{meas}[c]	0.102 (0.255)
Refinement Statistics	
resolution range (Å)	81.9–2.3 (2.36–2.3)
no. of reflections, $F(hkl) > 0$	48587
R-factor[d]	0.201 (0.248)
R_{free}[e]	0.255 (0.349)
rmsd for bonds (Å)	0.016
rmsd for angles (deg)	1.474
Ramachandran statistics (% of residues)	
allowed	89.6
additional	10.4
generous and disallowed	0.0

[a] Values in parentheses refer to those for the highest-resolution shell. [b] $R_{sym} = \sum_h\sum_i|I_i(hkl) - \langle I(hkl)\rangle|/\sum_h\sum_i I_i(hkl)$, where $I_i(hkl)$ is the *i*th measurement of reflection *hkl* and $\langle I(hkl)\rangle$ is the averaged value for the reflection. [c] R_{meas} is the multiplicity-weighted R_{sym}. [d] *R*-factor $= \sum_h||F_o(hkl)| - |F_c(hkl)||/\sum_h F_o(hkl)$, where F_o and F_c are the observed and calculated structure factor amplitudes for reflection *hkl*, respectively. [e] R_{free} is the *R*-factor calculated on a randomly chosen subset of reflections (1560 structure factors, 3.1% of total data) excluded from the minimization throughout refinement.

RESULTS AND DISCUSSION

Crystal Structure of the YeiK−Inosine Michaelis Complex. The structures of several group I NHs have been previously determined, but detailed experimental information about the NH−substrate contacts are still missing. Steady-state kinetics of YeiK showed that inosine is a poor substrate, characterized by a millimolar K_M and a low turnover number (Table 3). Taking advantage of this relatively slow conversion of inosine by YeiK (0.086 s^{-1}, corresponding to one turnover every 11.6 s), we cryotrapped at 100 K the YeiK−inosine complex and determined its crystal structure to 2.3 Å resolution. Electron density maps showed the presence of an active-site ligand only when the crystals were soaked for more than 30 s. The overall structure of YeiK is unaffected by binding of inosine (Figure 1A). One of the four independent YeiK subunits in the crystal displays the closed conformation, typical of group I NH enzymes bound to substrate-mimicking ligands (*9, 23*). The other three monomers instead display different degrees of flexibility in the $\beta3-\alpha3$ loop and $\alpha9$ helix, reminiscent of the open ligand-free or product-bound structures of NHs (*11, 22, 24*). The substrate binds as expected to the Ca^{2+}-containing active site in the catalytic cavity at the C-terminal end of the core β-sheet. The ribosyl moiety adopts a distorted C4′-endo conformation that confirms that ground-state destabilization is a driving force for NH catalysis. The hypoxanthine base is bound in a conformation that is intermediate between *syn* and *anti* ($\chi = 52°$, dihedral angle defined by atoms O4′, C1′, N9, and C4), with the C1′−C2′ bond of ribose substantially

Table 3: Effect of Mutations in Helix α9 Residues on the Steady-State Kinetic Parameters of the CU-NH YeiK with Uridine and Inosine Substrates

	uridine			inosine		
enzyme	k_{cat} (s^{-1})	K_M (mM)	k_{cat}/K_M (10^4 M^{-1} s^{-1})	k_{cat} (s^{-1})	K_M (mM)	k_{cat}/K_M (10^3 M^{-1} s^{-1})
YeiK	5.4 ± 0.2	0.12 ± 0.01	4.3 ± 0.3	0.086 ± 0.003	2.34 ± 0.32	0.037 ± 0.005
T223A	39.8 ± 1.6	0.33 ± 0.03	12.0 ± 1.2	0.180 ± 0.005	3.29 ± 0.22	0.055 ± 0.004
T223F	18.8 ± 0.6	0.31 ± 0.02	6.0 ± 0.5	0.109 ± 0.006	5.30 ± 0.60	0.021 ± 0.002
T223Y	44.3 ± 3.3	1.13 ± 0.11	3.9 ± 0.5	0.035 ± 0.001	1.16 ± 0.11	0.030 ± 0.003
Q227A	46.9 ± 1.3	0.77 ± 0.04	6.0 ± 0.3	0.182 ± 0.004	4.31 ± 0.21	0.042 ± 0.002
Q227F	52.5 ± 1.9	1.19 ± 0.07	4.4 ± 0.3	0.125 ± 0.003	1.77 ± 0.15	0.071 ± 0.01
Q227Y	15.1 ± 0.7	0.57 ± 0.04	2.6 ± 0.2	0.593 ± 0.015	2.14 ± 0.15	0.278 ± 0.02
T223F/Q227Y	59.1 ± 1.4	1.09 ± 0.07	5.4 ± 0.3	0.382 ± 0.011	4.42 ± 0.42	0.0864 ± 0.01
T223Y/Q227Y	72.9 ± 7.3	1.06 ± 0.14	6.8 ± 1.1	3.62 ± 0.12	1.93 ± 0.13	1.88 ± 0.14

coplanar with respect to the purine ring (Figure 1B). The aglycone is not fully defined in the electron density due to the catalysis that occurred within the crystal and was optimally refined with an occupancy of 70%. This partial occupancy may also explain the observed open structure in three YeiK monomers in the crystal. The hypoxanthine base is closely approached by the $\beta3-\alpha3$ loop, making extensive van der Waals contacts with the conserved residues Ile81 and His82.[2] In particular, the apolar contacts with the side chain atoms of Ile81 force the base in an axial conformation with respect to the ribose by reducing the conformational space available to the purine ring (Figure 1C). His82 instead approaches the five-membered ring of hypoxanthine in a T-shaped interaction that may provide additional binding energy (*25*). The purine ring also establishes van der Waals contact with the highly conserved Phe165 residue, as well as with Phe159. The terminal residue of helix α9, Tyr231, acts as a lid on top of the enzyme active site and closely approaches the purine base with the phenol ring carbons in an apparently unfavorable C−O van der Waals contact. Hydrogen bonding interactions are established between the hypoxanthine ring N7 and O6 atoms and the side chain amide group of Gln227. The phenolic oxygen of the Tyr231 side chain is also involved in polar contacts with the base N1 atom, providing additional binding energy. Although it cannot be established at the resolution of this structure, the interactions observed support a preferred tautomerization of the hypoxanthine ring toward the iminol form when bound to YeiK. Alternatively, inosine may be bound in the more represented keto tautomer, and the repulsive interactions between the Gln227 side chain carbonyl and O6 may account for its low affinity for YeiK. The side chain of His239, the residue proposed to act as a general acid in group I NHs, is 3.2 Å from the N7 atom of the hypoxanthine base. The imidazolium ring is in a perpendicular orientation with respect to the base ring that is unfavorable for proton transfer (Figure 1C). Mutation of His239 to alanine in the *Crithidia* IU-NH dramatically reduces the rate of inosine hydrolysis, and its contribution to catalysis amounts to −4.6 kcal/mol (*14*). The distance and geometry of this interaction in the Michaelis complex may prevent an efficient neutralization of the negative charge at the transition state and thus explain the slow turnover of inosine by YeiK.

[2] Because of the differences in the numbering of the amino acids in different group I NH enzymes, protein residues are numbered in this work according to the numbering of the pyrimidine nucleoside hydrolase YeiK sequence. For clarity, residues 223, 227, and 239 of YeiK correspond to Tyr225, Tyr229, and His241, respectively, in the *Crithidia* IU-NH. An alignment of the sequences at the α9 helices of the enzymes discussed in the text is provided in Figure 5.

We modeled a molecule of inosine into the active site of the *Crithidia* IU-NH, a group I NH that efficiently hydrolyzes purine nucleosides (Figure 2) in the same conformation that was observed in YeiK. In this enzyme, Gln227 is substituted with a tyrosine whose side chain hydroxyl closely approaches both the N7 and O6 atoms of hypoxanthine, with a high potential for retaining a hydrogen bonding interaction. Tyr231 of YeiK is replaced with an arginine, closing the top of the active-site cavity and within hydrogen bonding distance of the N1 atom of the base. A second tyrosine residue, replacing Thr223 of YeiK, is adequately positioned for establishing polar interactions with the purine N7 atom. This residue may provide hydrophobic binding interactions with the purine ring and is also interacting with both Tyr227 and His239 via its side chain hydroxyl. These four residues belong to the α9 helix that borders the NH active site and are not conserved in the pyrimidine-specific CU-NHs (*9*). Instead, both *Leishmania* and *Crithidia* IU-NHs display two tyrosines at positions 223 and 227 (Figure 2). Molecular dynamics studies suggested a possible role of Tyr227 in catalysis (*27*). We investigated whether the concomitant presence of two tyrosines at these sites is a requirement for IU-NH activity by enzymes belonging to NH homology group I.

A Double Mutation Converts the CU-NH YeiK into a IU-NH. To assess whether a single tyrosine in the α9 helix was sufficient to enhance the catalytic efficiency of YeiK toward purine nucleosides, we individually mutated residues Thr223 and Gln227 of the *E. coli* YeiK CU-NH to tyrosine. The T223Y mutation does not affect the specificity of the enzyme toward inosine or uridine, as a consequence of compensating variations in k_{cat} and K_M (Table 3). The Q227Y mutation instead has a strong, enhancing effect on the hydrolysis of inosine, and the catalytic efficiency (k_{cat}/K_M) for the purinic substrate is increased by a factor of 7.6, as a result of a specific increase in k_{cat}. This variation corresponds to an overall stabilization of the transition state of the hydrolytic cleavage of inosine by −1.2 kcal/mol, as judged from the variation of the pseudo second-order rate constant k_{cat}/K_M. To demonstrate a specific role for tyrosine residues at positions 223 and 227 in group I NHs in producing IU-NH-like activity, we also mutated these amino acids to alanine or phenylalanine. These mutations do not improve significantly the catalytic efficiency of YeiK toward inosine, with all variations to the overall $\Delta\Delta G^{\ddagger}$ being below $\pm k_B T$ and thus due to weak interactions (Figure 3). In particular, the Q227F mutant shows a 4-fold lower efficiency than the Q227Y mutant, confirming the role of this tyrosine hydroxyl in catalysis. The introduction of a Phe residue at position

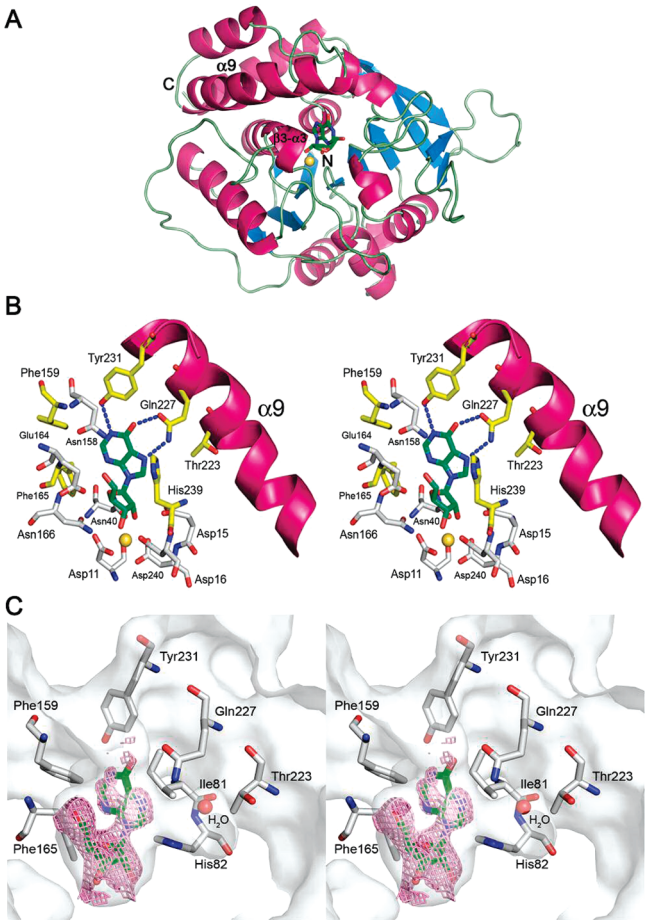

FIGURE 1: Structure of the YeiK−inosine Michaelis complex. (A) Group I NH fold, as represented by the monomer of the YeiK CU-NH from *E. coli* in complex with the substrate inosine. α-Helices are depicted as pink ribbons and β-strands as blue arrows, and the loop region is colored light green. For a detailed description of the fold topology, see ref (*22*). (B) Stereographic view of the catalytic-site cavity of the CU-NH YeiK from *E. coli*, including the active-site Ca^{2+} ion, a ribbon representation of the α9 helix, and the substrate inosine. Amino acids are shown as sticks, with the carbon atoms of the ribose-contacting residues colored gray and those of the base-contacting ones yellow. Carbon atoms of inosine are colored green, and putative hydrogen bonds between the protein and substrate are shown as dashed lines. (C) Tight fit of inosine to the YeiK active site. The inosine molecule is shown as a stick model together with the semitransparent molecular surface of YeiK. Amino acid residues contributing to the molecular surface in contact with the base are shown as sticks. The active site of YeiK complements the hypoxanthine ring and does not permit alternative conformations such as *syn* or *anti*. The omit ($2mF_o - DF_c$, φ_c) electron density of inosine contoured at 1.0σ is shown as a violet grid. This figure was generated with PyMol (http://pymol.sourceforge.net).

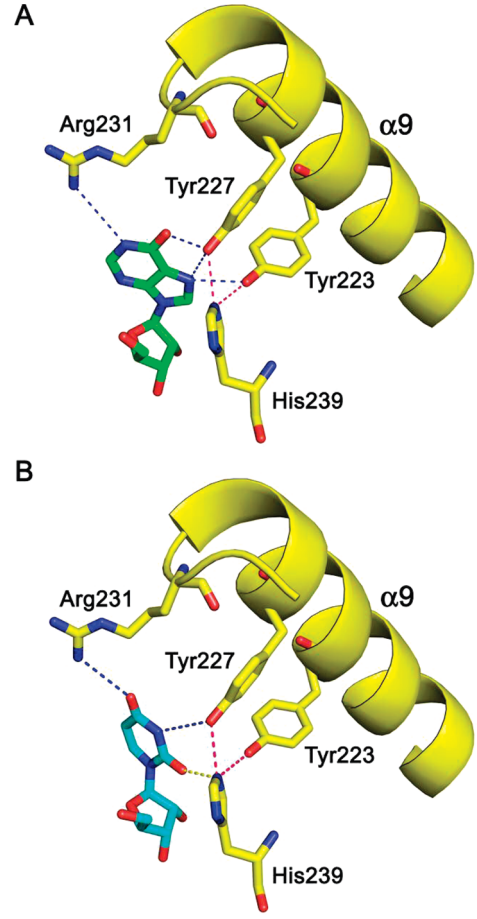

FIGURE 2: Comparison of substrate binding to the IU-NH from *C. fasciculata*. Cartoon representation of models of the active site of the IU-NH from *Crithidia* bound to (A) inosine and (B) uridine. The model in panel A was obtained by superposition of YeiK bound to inosine with the closed IU-NH structure observed in the complex with a transition-state-like inhibitor (*23*). The model in panel B was obtained on the basis of the inhibitor conformation in the IU-NH−pAPIR complex (*26*). Dashed blue lines represent possible hydrogen bonds between the enzyme and the base. Dashed pink lines depict the interactions between the residues of the Tyr-Tyr-His triad. Tyr227 is properly oriented for the formation of a hydrogen bond to the N7 atom of hypoxanthine. His239 is within the correct distance but is suboptimally oriented with respect to the acceptor atom. Instead, the O2 carbonyl of uridine is 2.7 Å from the side chain of His239 (dashed yellow line), and in a more favorable orientation for direct proton transfer. This figure was generated with PyMol (http://pymol.sourceforge.net).

223 severely impairs binding of substrate, suggesting that the bulky hydrophobic ring lacking a hydrogen bond donor or acceptor (such as the OH group in tyrosine) poses a steric constraint at the active site.

Finally, we engineered a T223Y/Q227Y double mutant (YY) to mimic the α9 helix of known IU-NHs. The YY enzyme displays a catalytic efficiency toward inosine that is more than 50-fold increased compared to that of wild-type YeiK. The K_M value for the substrate inosine is within experimental error compared to those of both wild-type YeiK and the Q227Y mutant. The enhanced transition-state stabilization is achieved through a more efficient chemical step, probably the consequence of an effective neutralization of the negative charge at the leaving purine base. The double mutation effectively lowers the energetic barrier for inosine hydrolysis by a total of −2.4 kcal/mol, thus indicating that the effect of the mutations on the catalytic efficiency of the enzyme is not additive; rather, the two tyrosines synergize to stabilize the transition state (Figure 3). The favorable interaction between the two tyrosine residues (1.8 kcal/mol) overcomes the unfavorable effect of the individual Tyr223 mutation on inosine hydrolysis. The kinetic analysis of double mutant T223F/Q227Y (FY) shows that the hydrophobic contribution from the residue at position 223 is not sufficient to achieve optimal catalysis. Indeed, the increase in catalytic efficiency for this mutant compared to the wild-type enzyme is approximately 2-fold, compared to 51 for the YY mutant. This limited enhancement could be ascribed to both an inefficient proton transfer and poor binding of the substrate, as judged from the k_{cat} and K_M values (Table

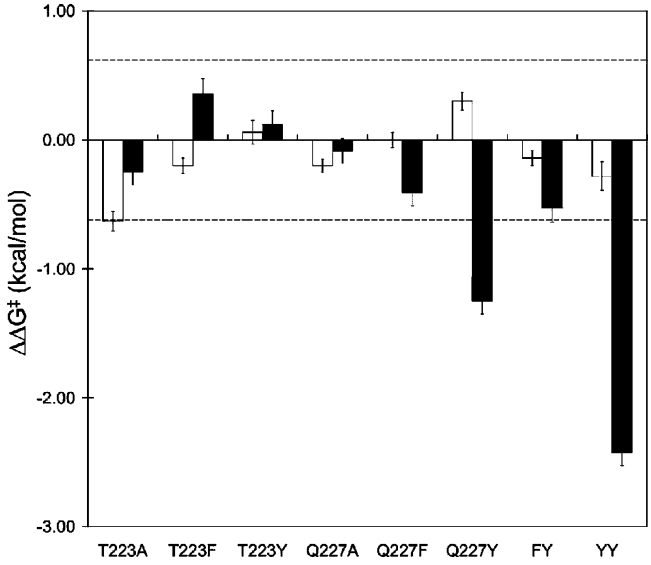

FIGURE 3: Effect of mutations on the YeiK-catalyzed hydrolysis of uridine (white bars) or inosine (black). The abscissa reports the different mutants, while the ordinate displays the $\Delta\Delta G^{\ddagger}$ state for each mutant, representing the variation in the free energy of the transition state of the enzyme-catalyzed reaction compared to wild-type YeiK. Values were calculated with the relation $\Delta\Delta G^{\ddagger}(\text{substrate}) = -RT \ln[\kappa_B(\text{substrate})/\kappa_A(\text{substrate})]$, where κ_A and κ_B are the catalytic efficiencies of the enzymes under comparison. Bars depict standard errors. The horizontal dashed lines intersect the ordinate axis at the values of $\pm k_B T$ at 37 °C (0.62 kcal/mol) and represent the thermal energy at the temperature of the enzymatic assay. Effects within these values can be ascribed to weak interactions that are comparable to the thermal motion of the protein atoms.

3). Hence, these results clearly demonstrate that the hydroxyl groups of residues Tyr223 and Tyr227 cooperate to establish an efficient binding site and facilitate the activation of the leaving group in the hydrolysis of inosine. The integrity of the Tyr-Tyr-His triad is pivotal for optimal hydrolysis of purine nucleosides by group I NHs.

All the mutations engineered at amino acids 223 and 227 of YeiK result in a large increase in k_{cat} with uridine as the substrate, paralleled by proportional increments in K_M, suggesting the introduction of a conformational strain on uridine that is beneficial for catalysis. Since diverse amino acid residues such as Ala, Phe, and Tyr have similar effects on K_M, the mutations could affect the conformational change that takes place between the ligand-free and substrate-bound forms of YeiK. Notably, the YY mutant lowers by comparable amounts the activation energy for both uridine and inosine substrates, with 15- and 40-fold increases in k_{cat}, respectively. Moreover, in this mutant, the 55-fold discrimination of YeiK in favor of uridine is reduced to 20-fold under saturating substrate conditions, implying an enhanced turnover of inosine through a more efficient chemical step.

The engineered YY YeiK mutant displays a catalytic efficiency toward inosine ($k_{cat}/K_M = 1.9 \times 10^3$ M^{-1} s^{-1}) approaching that of the IU-NHs from *C. fasciculata* (*9*), *Leishmania major* (*24*), and *Salmonella enterica* (*28*) that amount to 7.6×10^4, 2.7×10^5, and 1.4×10^4 M^{-1} s^{-1}, respectively. Indeed, the turnover number of YY ($k_{cat} = 3.6$ s^{-1}) favorably compares with those of the natural IU-NHs (119, 28, and 9 s^{-1}, respectively), but the K_M value is significantly higher (1.9 mM compared to 0.44, 0.36, and 0.65 mM, respectively), indicating suboptimal enzyme–substrate contacts under the rapid equilibrium hypothesis. This difference can readily be ascribed to the fine-tuning of the active-site environment deriving from evolutionary pressure in natural IU-NH enzymes. The YY mutant is a *bona fide* IU-NH, being also active toward the purine nucleoside adenosine, with a k_{cat} of 0.41 ± 0.04 s^{-1} and a K_M of 3.75 ± 0.15 mM. Finally, the nucleoside tubercidin (7-deazaadenosine) is hydrolyzed by the YY mutant at a rate of 0.013 s^{-1}, highlighting the role of the N7 atom of purines in the hydrolytic mechanism.

Leaving Group Activation in Purine and Pyrimidine Nucleosides. The catalytic mechanism of group I NHs largely relies on the distortion of the ribosyl moiety toward an oxonium ion geometry, enhancing its reactivity with a Ca^{2+}-polarized water molecule (*13, 23*). The negative charge developing at the leaving group nitrogenous base must be stabilized through either protonation or specific polar interactions. The rate of hydrolysis of nucleosides in solution shows a linear dependence with pH in the range of 0–7, suggesting the protonated base as the reactive species. Kinetic isotope effect studies of the *Crithidia* IU-NH-catalyzed hydrolysis of inosine also indicates a pre-transition-state protonation at the N7 atom (*13*). Structural and mutagenesis studies identified His239 as a likely candidate for proton transfer (*14*). Our study demonstrates the requirement of a specific network of residues for the protonation of the purine ring. This catalytic triad formed by residued Tyr223, Tyr227, and His239 is, however, not needed for the hydrolysis of pyrimidine nucleosides, being absent in all CU-NHs thus far characterized. Moreover, all single and double mutations of residues 223 and 227 of YeiK have a minimal effect on the rate of hydrolysis of uridine compared to the wild-type enzyme (Table 3). Hence, the hydrolytic cleavage of the N-glycosidic bond in purine or pyrimidine nucleosides catalyzed by nonspecific group I NH enzymes relies on different residues for leaving group activation. How can the same NH enzyme perform a dual role in nucleoside hydrolysis?

Purine and pyrimidine bases differ in their acid−base properties, and these differences are likely reflected in the mechanism of leaving group stabilization. As the NH-catalyzed hydrolysis of uridine proceeds along the reaction coordinate, a negative charge develops at the N1 atom of the base that can be delocalized to the O2 carbonyl. The N1−O2 imidate form of uracil has a pK_a of 9.8 and could be protonated by amino acid residues with a pK_a nearing neutral values, such as His239 in group I NHs. When a uridine molecule bound to the *Crithidia* IU-NH active site is modeled, the base O2 carbonyl is indeed placed within hydrogen bonding distance of His239 (Figure 4), suggesting a likely direct protonation by this residue. The transition-state structure of *E. coli* RihC-catalyzed hydrolysis of uridine supports the hypothesis of the importance of enzymatic interactions with the carbonyl O2 atom for base activation (*29*). Moreover, mutation of His239 to alanine in YeiK results in a 10-fold decrease in k_{cat}/K_M for the substrate uridine (*10*). Alternative mechanisms include the stabilization of the anionic form of the base by the enzyme via polar interactions. For instance, several lines of evidence indicate that an uracilate anion is the leaving group in the reaction catalyzed by the enzyme uracil DNA glycosidase (*30*). For this repair enzyme from *E. coli*, a single hydrogen bond to a neutral

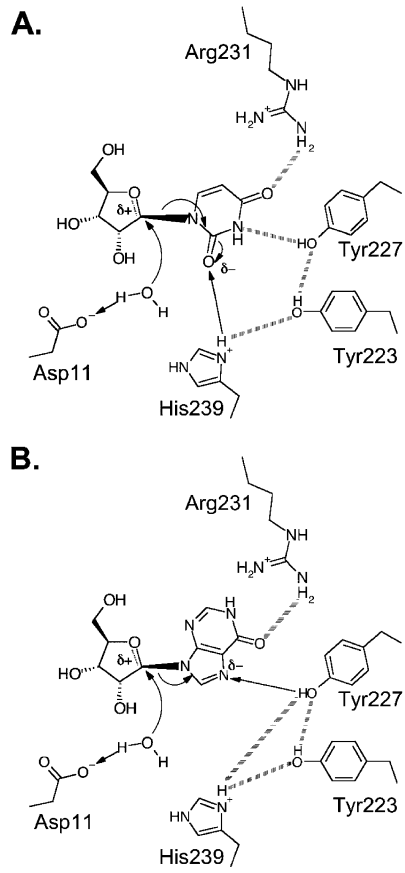

FIGURE 4: Proposed mechanism for the activation of the leaving groups in pyrimidine and purine nucleosides by group I NH enzymes. A common feature of the NH-catalyzed reaction inovolves the distortion of the ribosyl moiety of nucleosides toward an oxonium ion geometry, bearing a partial positive charge. Asp11 acts as a general base, removing a proton from an ordered water molecule and activating the nucleophile. Different active-site residues are involved in the neutralization of the developing negative charge at the nitrogenous base in purines or pyrimidines. The schemes represent the interactions between the IU-NH from *C. fasciculata* and the substrates (A) uridine and (B) inosine. (A) Residue His239, because of its proximity and favorable geometry, can directly transfer a proton to the carbonyl O2 atom of the leaving group uracil, neutralizing the negative charge. This mechanism is conserved in both IU- and CU-NH enzymes. (B) Instead, the proton required for activation of hypoxanthine is actively shuttled from His239 to the N7 atom of the purine ring via the Tyr227 side chain hydroxyl, while Tyr223 maintains the correct geometry of the triad and perhaps influences the hydroxyl pK_a.

histidine was shown to assist the uracilate anion stabilization by shifting the nitrogenous base pK_a to a value of 6.4. Hence, the uracil moiety of uridine could be similarly activated in the NH-catalyzed hydrolysis, achieving a stabilization of the negatively charged base via hydrogen bonding interactions. While further experiments are required to fully clarify such details of the NH-catalyzed hydrolysis of uridine, it is clear that, at least for the *E. coli* YeiK enzyme, residues Thr223 and Gln227 play a marginal role in stabilizing the transition state of the enzymatic reaction with uridine, with perhaps an effect on binding.

Inosine is a poor substrate for wild-type YeiK, but the engineering of a IU-NH-like Tyr-Tyr-His triad greatly augments the rate of enzymatic hydrolysis. Hypoxanthine has a markedly different acid−base behavior compared to uridine, with an acidic N7 atom (p$K_a \sim 2.3$) and two other basic sites at N1 (p$K_a = 9.9$) and N9 (p$K_a = 12.1$). As hydrolysis progresses, the negative charge developing at the ring increases the pK_a of N7, facilitating its protonation. On the basis of this structural analysis, Tyr227 can interact with N7 of inosine in IU-NHs while Tyr223 and His239 do not directly contact the base (Figure 4). The geometry of the catalytic triad is thus suggestive of a central role performed by Tyr227 in the neutralization of the negative charge. One possibility is that its side chain hydroxyl could act as a bridge between the protonated His239 and the purine base, with Tyr223 cooperating in directing proton transfer. Alternatively, the simultaneous presence of Tyr223 and His239 could perturb the side chain pK_a values, increasing the intrinsic propensity for proton transfer by Tyr227.

Our study further demonstrates how the base activation mechanism is markedly different in group I NHs from the one employed by the *Trypanosoma vivax* IAG-NH, belonging to homology group II. In this enzyme, aromatic ring stacking (*31*) and an intramolecular O5′−C8 hydrogen bond (*32*) favored by the *anti* conformation of the nitrogenous base cooperate in increasing the N7 pK_a to favor protonation of the leaving group directly from the solvent. Thus, group I and group II NHs share a common fold and strategy for ribosyl distortion and nucleophile activation in N-glycosidic bond hydrolysis but have evolved completely different mechanisms for promoting the departure of the nitrogenous base.

Deciphering Substrate Specificity from the Sequence of Group I NHs. NH-like proteins are annotated in protein databases on the basis of the presence of the N-terminal DXDXXXDD motif, involved in the binding of the catalytic-site Ca^{2+} ion. The nature of the residue immediately preceding the aspartate that completes the coordination sphere of the divalent cation (Asp240 in YeiK)[2] allows the distinction between purine-specific (group II) and either nonspecific or pyrimidine-specific NHs (group I) (*10*). Our identification of residues specifically involved in the hydrolysis of purine nucleosides defines further criteria that can be used to anticipate the substrate specificity of NHs. On the basis of these considerations, we analyzed the primary structures of NH-like proteins present in protein sequence databases (Figure 5). The majority of group I NHs in prokaryotes belong to the pyrimidine-specific CU-NH family, bearing a hydrophilic or charged amino acid corresponding to Gln227 of YeiK. This finding likely reflects a lesser need of purine nucleosidase activity in these organisms, since bacteria are generally capable of *de novo* purine synthesis. Moreover, the catabolism of nitrogenous bases is performed by efficient nucleoside phosphorylases (*1*). The analysis of the primary structure of NH-like proteins present in databases highlights the fact that putative IU-NHs, carrying both Tyr223 and Tyr227, are largely found in purine-auxotrophic protozoan parasites, such as *Leishmania*, where nucleoside phosphorylase activity is absent (*3*). However, nonspecific isozymes are also annotated in bacterial species (Figure 5). For instance, the IU-NH-like activity of the RihC proteins from *E. coli* and *S. enterica* has been previously characterized (*15, 28, 29*). Bacterial RihC homologues are peculiar in their α9 helix sequence, since they show a shorter segment between helices α8 and α9 (Figure 5). This region could hence display a different spatial arrangement of amino acid residues at the active site. Indeed, preliminary characterization of the structure of the RihC IU-NH from *E. coli* shows

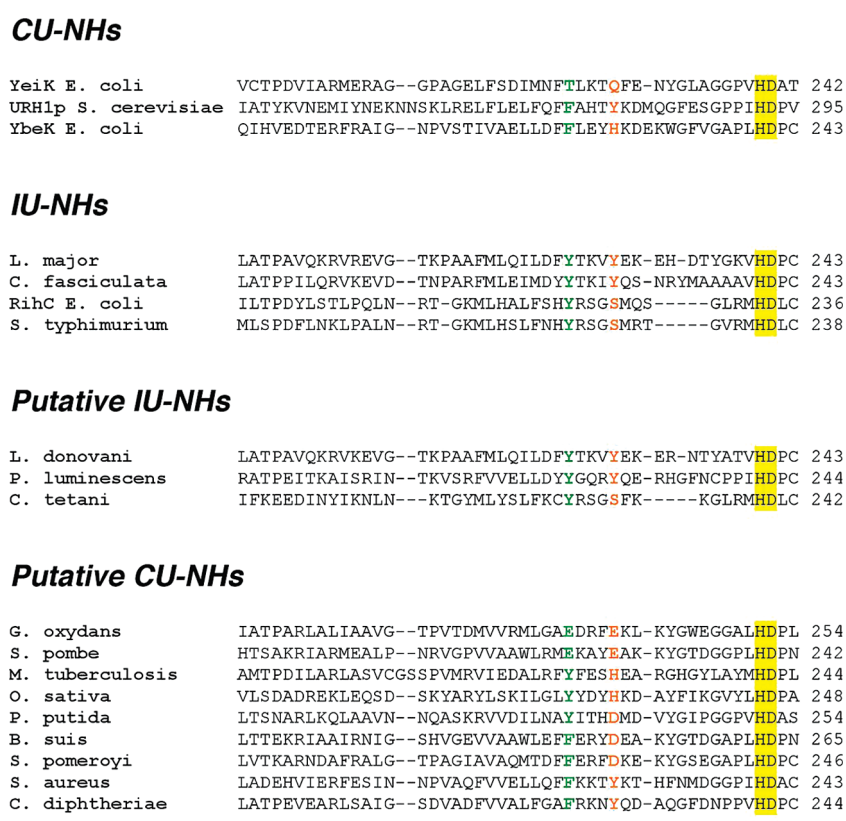

FIGURE 5: Primary structure alignment from the α9 helix region to the conserved His239 for group I NHs. The characterized CU-NHs and IU-NHs are aligned in the top part of the figure. Following, sample putative IU-NHs are annotated on the basis of the presence of either Tyr227 or Ser227 alone (bold orange typeface) in conjunction with Tyr223 (green). In the bottom part, putative CU-NHs are annotated on the basis of the absence of the complete catalytic triad. The numbering in the first row, corresponding to the primary structure of YeiK, is that followed throughout the text. The numbering of each sequence indicates the actual residue numbers for the corresponding protein.

that a Tyr223 homologue is indeed present, and Tyr227 is substituted with a serine (Figure 5) whose side chain hydroxyl establishes similar contacts with the neighboring residues (C. Minici and M. Degano, manuscript in preparation). Thus, it is conceivable that Tyr227 in IU-NHs could be substituted with a serine or threonine, provided that the shorter residue adequately approaches both the substrate and the other two components of the triad.

To further confirm that the described catalytic triad is essential for IU-NH-like activity, we characterized the group I NH protein found in the proteome of the yeast *S. cerevisiae*, encoded by the *urh1* gene. This putative yeast hydrolase lacks Tyr223 but maintains a Tyr227 residue (Figure 5). Given the strong, synergic effect deriving from the presence of all members of the catalytic triad, the *urh1* gene is thus expected to encode a CU-NH enzyme. A uridine hydrolase enzyme has been previously partially purified from yeast (*33*), and the overexpression in yeast cells of the *urh1* gene increases the nucleosidase activity on cytidine (*34*). URH1p is also involved in the conversion of both endogenous and exogenous nicotinamide ribonucleoside into nicotinamide and contributes to the cellular NAD^+ pool (*6*). A detailed enzymatic characterization of the yeast hydrolase has not yet been reported. We characterized a recombinant form of the *S. cerevisiae urh1* gene product. The URH1p protein differs from known group I structures in the quaternary assembly, being found in a 1:3 dimer:monomer ratio by size exclusion chromatography. We performed steady-state kinetic measurements on the purified, recombinant yeast NH. The enzyme is a uridine-preferring CU-NH ($k_{cat} = 117 \pm 21$ s^{-1}, $K_M = 0.63 \pm 0.07$ mM, and $k_{cat}/K_M = 1.86 \times 10^5$ M^{-1} s^{-1}), with lower specificity toward cytidine ($k_{cat} = 12 \pm 1.7$ s^{-1}, $K_M = 1.02 \pm 0.08$ mM, and $k_{cat}/K_M = 1.18 \times 10^4$ M^{-1} s^{-1}). As predicted from the absence of the Tyr-Tyr-His triad, inosine is indeed not a substrate for URH1p, with a k_{cat} of <0.001 s^{-1}.

CONCLUSIONS

In summary, in this work we show that the presence of two specific hydroxylated residues is a requirement for purine nucleoside hydrolase activity in members of NH homology group I. These amino acid residues cooperate with the trademark histidine in assembling a catalytic triad that is probably enhancing the process of proton transfer to the purinic moiety. Conversely, the hydrolysis of pyrimidine nucleosides requires primarily the presence of the catalytic histidine and is not affected by the nature of the residues in the α9 helix. This finding demonstrates that the same NH enzyme can plastically adapt to the chemical differences between substrates by using distinct amino acid residues at its active site. Our results provide for the first time a definition of the biochemical basis for the different substrate specificities by IU-NH and CU-NH enzymes.

ACKNOWLEDGMENT

We thank Prof. Silvano Geremia for helpful discussions on the cryotrapping experiments.

REFERENCES

1. Schramm, V. L. (1997) Enzymatic N-riboside scission in RNA and RNA precursors. *Curr. Opin. Chem. Biol. 1*, 323–331.

2. Versées, W., and Steyaert, J. (2003) Catalysis by nucleoside hydrolases. *Curr. Opin. Struct. Biol. 13*, 731–738.
3. Hammond, D. J., and Gutteridge, W. E. (1984) Purine and pyrimidine metabolism in the trypanosomatidae. *Mol. Biochem. Parasitol. 13*, 243–261.
4. Todd, S. J., Moir, A. J., Johnson, M. J., and Moir, A. (2003) Genes of *Bacillus cereus* and *Bacillus anthracis* encoding proteins of the exosporium. *J. Bacteriol. 185*, 3373–3378.
5. Ribeiro, J. M., and Valenzuela, J. C. (2003) The salivary purine nucleosidase of the mosquito *Aedes aegypti*. *Insect Biochem. Mol. Biol. 33*, 13–22.
6. Belenky, P., Racette, F. G., Bogan, K. L., McClure, J. M., Smith, J. S., and Brenner, C. (2007) Nicotinamide riboside promotes Sir2 silencing and extends lifespan via Nrk and Urh1/Pnp1/Meu1 pathways to NAD^+. *Cell 129*, 473–484.
7. Parkin, D. W. (1996) Purine-specific nucleoside *N*-ribohydrolase from *Trypanosoma brucei brucei*. Purification, specificity, and kinetic mechanism. *J. Biol. Chem. 271*, 21713–21719.
8. Versées, W., Decanniere, K., Pellé, R., Depoorter, J., Brosens, E., Parkin, D. W., and Steyaert, J. (2001) Structure and function of a novel purine specific nucleoside hydrolase from *Trypanosoma vivax*. *J. Mol. Biol. 307*, 1363–1379.
9. Parkin, D. W., Horenstein, B. A., Abdulah, D. R., Estupiñan, B., and Schramm, V. L. (1991) Nucleoside Hydrolase from *Crithidia fasciculata*. Metabolic role, purification, specificity, kinetic mechanism. *J. Biol. Chem. 266*, 20658–20665.
10. Giabbai, B., and Degano, M. (2004) Crystal structure to 1.7 Å of the *Escherichia coli* pyrimidine nucleoside hydrolase YeiK, a novel candidate for cancer gene therapy. *Structure 12*, 739–749.
11. Estupiñan, B., and Schramm, V. L. (1994) Guanosine-inosine-preferring nucleoside *N*-glycohydrolase from *Crithidia fasciculata*. *J. Biol. Chem. 269*, 23068–23073.
12. Muzzolini, L., Versées, W., Tornaghi, P., Van Holsbeke, E., Steyaert, J., and Degano, M. (2006) New insights into the mechanism of nucleoside hydrolases from the crystal structure of the *Escherichia coli* YbeK protein bound to the reaction product. *Biochemistry 45*, 773–782.
13. Horenstein, B. A., Parkin, D. W., Estupiñan, B., and Schramm, V. L. (1991) Transition-state Analysis of Nucleoside Hydrolase from *Crithidia fasciculata*. *Biochemistry 32*, 7089–7097.
14. Gopaul, D. N., Meyer, S. L., Degano, M., Sacchettini, J. C., and Schramm, V. L. (1996) Inosine-uridine nucleoside hydrolase from *Crithidia fasciculata*. Genetic characterization, crystallization, and identification of histidine 241 as a catalytic site residue. *Biochemistry 35*, 5963–5970.
15. Petersen, C., and Møller, L. B. (2001) The RihA, RihB, and RihC ribonucleoside hydrolases of *Escherichia coli*. Substrate specificity, gene expression, and regulation. *J. Biol. Chem. 276*, 884–894.
16. Giabbai, B., and Degano, M. (2004) Cloning, purification, crystallization and X-ray analysis of the *Escherichia coli* pyrimidine nucleoside hydrolase YeiK. *Acta Crystallogr. D60*, 524–527.
17. Weiner, M. P., Costa, G. L., Schoettlin, W., Cline, J., Mathur, E., and Bauer, J. C. (1994) Site-directed mutagenesis of double-stranded DNA by the polymerase chain reaction. *Gene 151*, 119–123.
18. Kabsch, W. (1993) Automatic processing of rotation diffraction data from crystals of initially unknown symmetry and cell constants. *J. Appl. Crystallogr. 21*, 67–71.
19. Vagin, A. A., and Isupov, M. N. (2001) Spherically averaged phased translation function and its application to the search for molecules and fragments in electron-density maps. *Acta Crystallogr. D57*, 1451–1456.
20. Murshudov, G. N., Vagin, A. A., and Dodson, E. J. (1997) Refinement of macromolecular structures by the maximum-likelihood method. *Acta Crystallogr. D53*, 240–255.
21. Emsley, P., and Cowtan, K. (2004) Coot: Model building tools for molecular graphics. *Acta Crystallogr. D60*, 2126–2132.
22. Degano, M., Gopaul, D. N., Scapin, G., Schramm, V. L., and Sacchettini, J. C. (1996) Three-dimensional structure of the inosine-uridine nucleoside N-ribohydrolase from *Crithidia fasciculata*. *Biochemistry 35*, 5971–5981.
23. Degano, M., Almo, S. C., Sacchettini, J. C., and Schramm, V. L. (1998) Trypanosomal nucleoside hydrolase. A novel mechanism from the structure with a transition-state inhibitor. *Biochemistry 37*, 6277–6285.
24. Shi, W., Schramm, V. L., and Almo, S. C. (1999) Nucleoside hydrolase from *Leishmania major*. Cloning, expression, catalytic properties, transition state inhibitors, and the 2.5-Å crystal structure. *J. Biol. Chem. 274*, 21114–21120.
25. Burley, S. K., and Petsko, G. A. (1985) Aromatic-aromatic interaction: A mechanism of protein structure stabilization. *Science 229*, 23–28.
26. Fornili, A., Sironi, M., and Degano, M. (2007) Accurate description of nitrogenous base flexibility in classical molecular dynamics simulations of nucleotides bound to proteins. *J. Phys. Chem. B 111*, 6297–6302.
27. Mazumder, D., and Bruice, T. C. (2002) Exploring nucleoside hydrolase catalysis in silico: Molecular dynamics study of enzyme-bound substrate and transition state. *J. Am. Chem. Soc. 124*, 14591–14600.
28. Hansen, M. R., and Dandanell, G. (2005) Purification and characterization of RihC, a xathosine-inosine-uridine-adenosine-preferring hydrolase from *Salmonella enterica* serovar Typhimurium. *Biochim. Biophys. Acta 1723*, 55–62.
29. Hunt, C., Gillani, N., Farone, A., Rezaei, M., and Kline, P. C. (2005) Kinetic isotope effects of nucleoside hydrolase from *Escherichia coli*. *Biochim. Biophys. Acta 1751*, 140–149.
30. Werner, R. M., and Stivers, J. T. (2000) Kinetic isotope effect studies of the rection catalyzed by uracil DNA glycosidase: Evidence for an oxycarbenium ion-uracilate anion intermediate. *Biochemistry 39*, 13241–13250.
31. Versées, W., Loverix, S., Vandemeulebrucke, A., Geerlings, P., and Steyaert, J. (2004) Leaving group activation by aromatic stacking: An alternative to general acid catalysis. *J. Mol. Biol. 338*, 1–6.
32. Loverix, S., Geerlings, P., McNaughton, M., Augustyns, K., Vandemeulebroucke, A., Steyaert, J., and Versées, W. (2005) Substrate-assisted leaving group activation in enzyme-catalyzed N-glycosidic bond cleavage. *J. Biol. Chem. 280*, 14799–14802.
33. Magni, G., Fioretti, E., Ipata, P. L., and Natalini, P. (1975) Baker's yeast uridine nucleosidase. Purification, composition, and physical and enzymatic properties. *J. Biol. Chem. 250*, 9–13.
34. Kurtz, J. E., Exinger, F., Erbs, P., and Jund, R. (2002) The URH1 uridine ribohydrolase of *Saccharomyces cerevisiae*. *Curr. Genet. 41*, 132–141.

BI702448S